ISSN 1070-3284, Russian Journal of Coordination Chemistry, 2022, Vol. 48, No. 12, pp. 924–934. © Pleiades Publishing, Ltd., 2022.

Double Pseudopolymeric $[Au\{S_2CN(CH_2)_5\}_2]_2[Ag_2Cl_4]\cdot CH_2Cl_2$ Complex: Preparation, Principles of Supramolecular Self-Assembly, Thermal Behavior, and Biological Activity against *Mycolicibacterium smegmatis* Strain

E. V. Korneeva[a], I. A. Lutsenko[b], O. B. Bekker[c], K. L. Isakovskaya[d, e], and A. V. Ivanov[a, *]

[a] *Institute of Geology and Nature Management, Far Eastern Branch of the Russian Academy of Sciences, Blagoveshchensk, 675000 Russia*

[b] *Kurnakov Institute of General and Inorganic Chemistry, Russian Academy of Sciences, Moscow, 119991 Russia*

[c] *Vavilov Institute of General Genetics, Russian Academy of Sciences, Moscow, 119991 Russia*

[d] *Nesmeyanov Institute of Organoelement Compounds, Russian Academy of Sciences, Moscow, 119991 Russia*

[e] *Mendeleev University of Chemical Technology of Russia, Moscow, 125047 Russia*

**e-mail: alexander.v.ivanov@chemist.com*

Received May 13, 2022; revised July 6, 2022; accepted July 6, 2022

Abstract—The double Au(III)–Ag(I) complex crystallizing as the solvated form of $[Au\{S_2CN(CH_2)_5\}_2]_2[Ag_2Cl_4]\cdot CH_2Cl_2$ (**I**) was obtained by the reaction of silver(I) *N*,*N*-pentamethylenedithiocarbamate with a solution of $Na[AuCl_4]$/5.15 M NaCl. According to X-ray diffraction data (CIF file CCDC no. 2062810), the structural units of the compound are nonequivalent $[Au\{S_2CN(CH_2)_5\}_2]^+$ cations (noncentrosymmetric *A* and centrosymmetric *B* and *C* in a ratio of 2 : 1 : 1), cyclic tetrachlorodiargentate(I) anions, $[Ag_2Cl_4]^{2-}$, and solvating CH_2Cl_2 molecule. The latter is retained in the structure due to two nonequivalent C–H···Cl hydrogen bonds formed with the cyclic $[Ag_2Cl_4]^{2-}$ anion involving its terminal Cl(1) and bridging Cl(2) chlorine atoms. The supramolecular self-organization of **I** is based on a system of multiple Ag···S and Cl···S secondary interactions that combine the ionic structural units of the complex into an intricate two-dimensional pseudopolymer layer. A study of the thermal behavior of **I** by simultaneous thermal analysis established the conditions for quantitative reduction of bound gold(III) and silver(I). The studied Au(III)–Ag(I) compound exhibits a high level of biological activity against the nonpathogenic *M. smegmatis* strain.

Keywords: double gold(III)–silver(I) complexes, pseudopolymer compounds, supramolecular self-assembly, Ag···S and Cl···S secondary interactions and C–H···Cl hydrogen bonds, thermal behavior, anti-tuberculosis activity

DOI: 10.1134/S1070328422700063

INTRODUCTION

Silver(I) complexes behave as corrosion inhibitors [1] and catalysts [2, 3] and can also be used as precursors of films and acanthite nanoparticles (α-Ag_2S) possessing semiconductor properties [4, 5], and for the design of chemosensors [6]. In addition, high biological activity of silver allows combining silver compounds with drugs used in medical practice (isoniazid) to increase the drug efficacy against *Mycobacterium tuberculosis* [7]. Silver(I) dithiocarbamate complexes form supramolecular structures stabilized by various types of secondary interactions [8–17]. Previously, we established the ability of silver(I) dialkyl(alkylene)dithiocarbamates to efficiently concentrate Au(III) from NaCl solutions to the solid phase to give ionic type Au(III)–Ag(I) pseudopolymers with intricately organized supramolecular structures [16, 18–20]. Compounds of this type are potential precursors of Janus nanoparticles of Ag_2S/Ag [21] and Ag_2S/Au [22] types. In continuation of these studies, we obtained here the double Au(III)–Ag(I) dithiocarbamato-chlorido complex of $[Au\{S_2CN(CH_2)_5\}_2]_2[Ag_2Cl_4]\cdot CH_2Cl_2$ (**I**) and studied the composition, supramolecular architecture, and the thermal behavior of this complex by IR spectroscopy, X-ray diffraction analysis, and simultaneous thermal analysis (STA). The biological activity of **I** was studied in vitro against nonpathogenic *M. smegmatis*, which is the model strain for *M. tuberculosis*.

EXPERIMENTAL

Sodium *N*,*N*-pentamethylenedithiocarbamate was prepared by the reaction of carbon disulfide (Merck)

with pentamethyleneimine (Aldrich) in alkaline medium [23]. Silver(I) *N*,*N*-pentamethylenedithiocarbamate was obtained by precipitation of silver(I) ions from a solution of $AgNO_3$ with an aqueous solution of $Na\{S_2CN(CH_2)_5\}\cdot 2H_2O$. For the preparation of 100 mg of silver(I) complex, a solution of $AgNO_3$ (0.063 g, 0.373 mmol) in water (50 mL) was added with stirring to a solution of $Na\{S_2CN(CH_2)_5\}\cdot 2H_2O$ (0.082 g, 0.373 mmol) in water (50 mL). The identity of the initial sodium salt and preparatively isolated silver(I) complex was confirmed by IR spectroscopy:

$Na\{S_2CN(CH_2)_5\}\cdot 2H_2O$ (ATR; ν, cm^{-1}): 3355 n.m, 3189 n.m, 2995 w, 2931 n.m, 2852 w, 1623 m, 1468 m, 1418 s, 1355 w, 1272 w, 1217 vs, 1107 m, 1071 w, 1004 w, 962 vs, 880 s, 854 vw, 613 m, 514 vs, 469 n.s.

$[Ag\{S_2CN(CH_2)_5\}]$ (ATR; ν, cm^{-1}): 2996 vw, 2933 n.m, 2850 n.m, 1471 s, 1426 vs, 1350 w, 1274 w, 1224 vs, 1108 m, 1074 vw, 1002 m, 950 s, 878 s, 613 w, 558 w, 510 m, 460 w.

Double bis(*N*,*N*-pentamethylenedithiocarbamato-*S*,*S*')gold(III) tetrachlorodiargentate(I) was prepared by the reaction of freshly precipitated silver(I) dithiocarbamate with a solution of $AuCl_3$/5.15 M NaCl (which is close to saturation conditions at 20°C).

Synthesis of I. A solution of $Na[AuCl_4]$ (10 mL) containing gold(III) (36.7 mg, 0.186 mmol) was added to $[Ag\{S_2CN(CH_2)_5\}]\}$ (100 mg, 0.373 mmol), and the mixture was stirred for 1 h at 60°C. The reaction of green-yellow precipitate with the solution is accompanied by rapid color change to orange and then to yellow-orange, while the working solution decolorized. The gold recovery from the solution to the solid phase was 95.6%, which indicates the formation of new compounds in the system. (The residual gold content in the solution after extraction was determined on a 1st class Hitachi atomic absorption spectrometer, model 180−50.)

The reaction of the synthesis of **I** can be represented as follows:

$$4[Ag\{S_2CN(CH_2)_5\}] + 2Na[AuCl_4] = [Au\{S_2CN(CH_2)_5\}_2]_2[Ag_2Cl_4]\ (\mathbf{I}) + 2Na[AgCl_2].$$

The resulting yellow-orange precipitate was collected on a filter, dried on the filter, and washed again with a minimum volume of water to remove water-soluble impurities. For the X-ray diffraction experiment, transparent needle orange crystals of solvated form of **I** were grown from dichloromethane; the yield was 70.7%.

For $C_{25}H_{42}N_4S_8Cl_6Ag_2Au_2$

Anal. calcd., %	C, 20.32	H, 2.86	N, 3.79
Found, %	C, 20.66	H, 2.60	N, 3.74

IR (ATR; ν, cm^{-1}): 2943 n.m, 2853 m, 1543 vs, 1435 vs, 1353 m, 1278 m, 1260 s, 1229 vs, 1132 m, 1111 s, 1002 vs, 945 m, 883 s, 852 s, 722 vs, 695 s, 625 m, 550 m, 508 m, 463 w, 452 w, 429 vw, 414 vs.

Elemental analysis was carried out on an automatic Carlo Erba EA 1108 C,H,N-analyzer. IR spectra were recorded on a Perkin-Elmer Spectrum 65 FT-IR spectrometer by the attenuated total reflectance (ATR) method in the 400–4000 cm^{-1} frequency range.

X-ray diffraction study of compound **I** was carried out at 120 K on a Bruker Apex II DUO diffractometer (CCD detector, MoK_α, λ = 0.71073 Å, graphite monochromator). The structure was solved using the ShelXT program [24] and refined by the full-matrix least squares method using the Olex2 program [25] in the anisotropic approximation for nonhydrogen atoms. The positions of hydrogen atoms were calculated geometrically and refined in the isotropic approximation in the riding model. The main crystallographic data and structure refinement details are summarized in Table 1, and selected bond lengths and angles are in Table 2.

The full set of X-ray diffraction parameters for complex **I** was deposited with the Cambridge Crystallographic Data Centre (CCDC no. 2062810; http://www.ccdc.cam.ac.uk/).

The thermal behavior of I was studied by simultaneous thermal analysis (STA) including parallel recording of thermogravimetry (TG) and differential scanning calorimetry (DSC) curves. The study was performed on an STA 449C Jupiter instrument (NETZSCH) in corundum crucibles covered by lids with holes to ensure a vapor pressure of 1 atm during thermal decomposition of samples. The samples were heated under argon to 1100°C at a heating rate of 5°C/min. The sample mass was 1.833–11.143 mg. The accuracy of temperature measurement was ±0.9°C, that for mass measurement was $\pm 1 \times 10^{-4}$ mg. For recording TG and DSC curves, a correction file was used, as well as temperature and sensitivity calibrations for the specified temperature program and heating rate. The independent determination of melting points was carried out on a PTP(M) instrument (OJSC Khimlaborpribor).

The biological activity of **I** was measured in the paper disc assay with *M. smegmatis mc² 155* strain. The growth inhibition zone was determined for a bacterial strain seeded by a lawn on an agarized medium around paper discs containing the test compound in various concentrations. The bacteria washed from Petri dishes with M-290 Trypton soy agar medium (Himedia) were grown overnight in Lemco-TW liquid medium (Lab Lemco' Powder 5 g L^{-1} (Oxoid), Peptone special 5 g L^{-1} (Oxoid), NaCl 5 g L^{-1}, Tween-80) at 37°C up to the mid logarithmic growth phase with the optical density OD600 = 1.5, mixed with melted

agarized M-290 medium in 1 : 9 : 10 ratio (culture : Lemco-TW : M-290). The culture was incubated for 24 h at 37°C. The concentration of the test compound providing the minimum growth inhibition zone was taken as minimal inhibitory concentration (MIC). The *M. smegmatis* system has a higher antibiotic and anti-tuberculosis drug resistance than *M. tuberculosis*; therefore, the selection criterion is the compound concentration <100 μg per disc. The assay includes quantitative measurement of the diameter of the inhibition zone of the *M. smegmatis* grown on the agarized medium around paper discs impregnated with the test compound. The compound was applied on the discs in various concentrations and the diameter of the halo (growth inhibition zone) was measured. The activity of the compound was determined relative to rifampicin (Rif), first-line drug for the treatment of tuberculosis.

RESULTS AND DISCUSSION

In the IR spectrum of complex **I**, mention should be made of the strong absorption band at 1543 cm^{-1}, important for characterization of Dtc ligands, which corresponds to N–C stretching vibrations in the Dtc moieties, ν(N–CS_2). This band is shifted to higher frequency in comparison to those of the initial silver(I) complex [Ag{$S_2CN(CH_2)_5$}] (1426 cm^{-1}) and the corresponding sodium salt Na(S_2CNPm)·$2H_2O$ (1418 cm^{-1}). All of these values are in the range between the vibrational frequencies of single N–C (1350–1250 cm^{-1}) and double N=C (1690–1640 cm^{-1}) bonds, which reflects the considerable contribution of double bond character to the formally single N–C(S)S bonds. However, according to IR spectroscopy data, the largest contribution is expected for complex **I**.

The strong band at 1111 cm^{-1} corresponds to the ν_{as}(C–S) asymmetric stretching modes, while highly intense band at 1002 cm^{-1} should be assigned to the ν_s(C–S) symmetric stretching modes. The medium-intensity absorption bands at 2943 and 2853 cm^{-1} are due to the $\nu_{as}(CH_2)$ and $\nu_s(CH_2)$ stretching vibrations in the piperidine heterocycle; the δ_s bending vibrations of the $-CH_2-$ groups give rise to a band at 1435 cm^{-1}. The CH_2Cl_2 solvate molecules account for the IR absorption bands corresponding to the C–Cl stretching modes [26]: 722 cm^{-1} ν_{as}(C–Cl) and 695 cm^{-1} ν_s(C–Cl). Both bands are shifted to lower frequencies with respect to those of individual CH_2Cl_2 [14], which is attributable to the participation of the solvate molecules of complex **I** in the intermolecular interactions.

The unit cell of the solvated ionic compound **I** contains two $[Au\{S_2CN(CH_2)_5\}_2]_2[Ag_2Cl_4]\cdot CH_2Cl_2$ formula units (Table 1). The structural parts of the complex are the $[Au\{S_2CN(CH_2)_5\}_2]^+$ cations, $[Ag_2Cl_4]^{2-}$ anions, and the CH_2Cl_2 solvate molecules (Fig. 1).

Table 1. Crystallographic data and X-ray experiment and structure refinement details for **I**

Parameter	Value
Molecular formula	$C_{25}H_{42}N_4S_8Cl_6Ag_2Au_2$
M	1477.48
System	Triclinic
Space group	$P\bar{1}$
a, Å	9.8395(5)
b, Å	14.9780(7)
c, Å	16.2788(8)
α, deg	67.1550(10)
β, deg	85.0610(10)
γ, deg	74.7090(10)
V, $Å^3$	2132.29(18)
Z	2
ρ(calcd.), g/cm^3	2.301
μ, (MoK_α), cm^{-1}	85.58
F(000)	1404
Crystal size, mm	0.35 × 0.05 × 0.05
Data collection range for θ, deg	2.146–26.999
Ranges of reflection indices	$-12 \le h \le 12$, $-19 \le k \le 19$, $-20 \le l \le 20$
Number of measured reflections	22959
Number of unique reflections (R_{int})	9311 (0.0513)
Number of reflections with $I > 2\sigma(I)$	7481
Number of refined parameters	427
GOOF	0.891
R-factors on $F^2 > 2\sigma(F^2)$	$R_1 = 0.0340$, $wR_2 = 0.0722$
R-factors for all reflections	$R_1 = 0.0476$, $wR_2 = 0.0788$
Residual electron density (min/max), $e/Å^3$	−1.25/1.22

The cationic part includes nonequivalent gold(III) complex ions: noncentrosymmetric *A* with Au(1) atom and centrosymmetric *B* and *C* with Au(2) and Au(3) atoms, respectively, in the 2 : 1 : 1 ratio. In each of the discussed cations, the nearly S,S'-isobidentate coordination of the pentamethylenedithiocarbamate (S_2CNPm) ligands (Fig. 1, Table 2) is accompanied by the formation of two four-membered [AuS_2C] metallacycles, which are linked by the gold atom to form bicyclic [CS_2AuS_2C] system. Thus, the central gold atom generates a fourfold, square-planar environment of sulfur atoms: the SAuS diagonal angles in the [AuS_4] polygon amount to 180° (cations *B* and *C*) or

Table 2. Selected bond lengths (*d*) and bond (ω) and torsion (φ) angles in the structure of **I***

Bond	*d*, Å	Bond	*d*, Å
Cation *A*			
Au(1)–S(1)	2.3379(1)	S(4)–C(7)	1.739(6)
Au(1)–S(2)	2.3448(1)	N(1)–C(1)	1.309(7)
Au(1)–S(3)	2.3448(1)	N(1)–C(2)	1.480(7)
Au(1)–S(4)	2.3451(1)	N(1)–C(6)	1.467(8)
S(1)–C(1)	1.745(6)	N(2)–C(7)	1.291(7)
S(2)–C(1)	1.737(6)	N(2)–C(8)	1.483(7)
S(3)–C(7)	1.743(6)	N(2)–C(12)	1.472(8)
Cation *B*		Cation *C*	
Au(2)–S(5)	2.3415(1)	Au(3)–S(7)	2.3428(1)
Au(2)–S(6)	2.3427(1)	Au(3)–S(8)	2.3367(1)
S(5)–C(13)	1.755(6)	S(7)–C(19)	1.732(6)
S(6)–C(13)	1.729(6)	S(8)–C(19)	1.742(6)
N(3)–C(13)	1.302(7)	N(4)–C(19)	1.299(7)
N(3)–C(14)	1.477(7)	N(4)–C(20)	1.481(8)
N(3)–C(18)	1.479(7)	N(4)–C(24)	1.479(8)
Angle	ω, deg	Angle	ω, deg
Cation *A*			
S(1)Au(1)S(2)	75.18(5)	Au(1)S(1)C(1)	87.0(2)
S(1)Au(1)S(3)	104.38(5)	Au(1)S(2)C(1)	87.0(2)
S(1)Au(1)S(4)	177.47(5)	Au(1)S(3)C(7)	87.39(19)
S(2)Au(1)S(3)	179.56(6)	Au(1)S(4)C(7)	87.5(2)
S(2)Au(1)S(4)	105.46(5)	S(1)C(1)S(2)	110.3(3)
S(3)Au(1)S(4)	74.99(5)	S(3)C(7)S(4)	110.1(3)
Cation *B*		Cation *C*	
S(5)Au(2)S(6)	75.55(5)	S(7)Au(3)S(8)	75.41(5)
S(5)Au(2)S(6)[a]	104.45(5)	S(7)Au(3)S(8)[b]	104.59(5)
Au(2)S(5)C(13)	86.5(2)	Au(3)S(7)C(19)	86.8(2)
Au(2)S(6)C(13)	87.06(19)	Au(3)S(8)C(19)	86.8(2)
S(5)C(13)S(6)	110.9(3)	S(7)C(19)S(8)	110.9(3)
Angle	φ, deg	Angle	φ, deg
Cation *A*			
Au(1)S(1)S(2)C(1)	−171.7(4)	Au(1)S(3)S(4)C(7)	178.0(4)
S(1)Au(1)C(1)S(2)	−172.5(3)	S(3)Au(1)C(7)S(4)	178.2(3)
S(1)C(1)N(1)C(2)	−173.9(5)	S(3)C(7)N(2)C(8)	2.6(9)
S(1)C(1)N(1)C(6)	5.7(9)	S(3)C(7)N(2)C(12)	177.2(5)
S(2)C(1)N(1)C(2)	6.4(9)	S(4)C(7)N(2)C(8)	−177.0(5)
S(2)C(1)N(1)C(6)	−174.0(5)	S(4)C(7)N(2)C(12)	−2.4(9)
Cation *B*		Cation *C*	
Au(2)S(5)S(6)C(13)	179.4(4)	Au(3)S(7)S(8)C(19)	−176.5(4)
S(5)Au(2)C(13)S(6)	179.4(3)	S(7)Au(3)C(19)S(8)	−176.9(4)
S(5)C(13)N(3)C(14)	−176.6(5)	S(7)C(19)N(4)C(20)	−4.5(9)
S(5)C(13)N(3)C(18)	−0.2(8)	S(7)C(19)N(4)C(24)	179.4(5)
S(6)C(13)N(3)C(14)	5.7(9)	S(8)C(19)N(4)C(20)	175.9(5)
S(6)C(13)N(3)C(18)	−177.9(4)	S(8)C(19)N(4)C(24)	−0.2(9)

Table 2. (Contd.)

Anion			
Bond	*d*, Å	Bond	*d*, Å
Ag(1)–Cl(1)	2.4175(17)	Ag(2)–Cl(4)	2.4140(16)
Ag(1)–Cl(2)	2.5293(16)	Ag(1)···Ag(2)	3.2187(7)
Ag(1)–Cl(3)	2.5710(16)	Ag(1)···S(1)	2.9456(15)
Ag(2)–Cl(2)	2.6204(17)	Ag(2)···S(2)[c]	3.1833(15)
Ag(2)–Cl(3)	2.5518(16)	Ag(2)···S(3)	3.0055(15)
Angle	ω, deg	Angle	ω, deg
Cl(1)Ag(1)Cl(2)	129.40(6)	Ag(2)Cl(3)Ag(1)	77.85(5)
Cl(1)Ag(1)Cl(3)	124.88(6)	Cl(1)Ag(1)···Ag(2)	160.21(5)
Cl(2)Ag(1)Cl(3)	103.00(5)	Cl(4)Ag(2)···Ag(1)	169.26(4)
Cl(3)Ag(2)Cl(2)	101.01(5)	Cl(1)Ag(1)···S(1)	93.84(5)
Cl(4)Ag(2)Cl(2)	124.68(5)	Cl(2)Ag(1)···S(1)	113.22(5)
Cl(4)Ag(2)Cl(3)	134.07(6)	Cl(3)Ag(1)···S(1)	77.54(5)
Ag(1)Cl(2)Ag(2)	77.35(5)	Au(1)S(1)···Ag(1)	111.94(6)
Angle	φ, deg	Angle	φ, deg
Ag(1)Cl(2)Cl(3)Ag(2)	–169.34(9)	Cl(2)Ag(1)Ag(2)Cl(3)	–171.40(7)

* Symmetry codes: [a] $1-x, -y, 1-z$; [b] $1-x, 2-y, -z$; [c] $-1+x, y, z$.

nearly 180° (cation *A*: 179.56° and 177.47°), which is indicative of a low-spin intraorbital dsp^2 hybrid state of gold(III). Despite their significant structural similarities, the nonequivalent cations show reliable structural differences in their respective geometric parameters; hence, they can be considered as conformational isomers.

The Au–C interatomic distances (2.834–2.857 Å) are markedly shorter than the sum of the van der Waals radii of these atoms: 3.36 Å [27, 28]; this illustrates small size of the rings, which are structurally stabilized due to π-electron density delocalization inside the rings. In turn, the AuSSC and SAuCS torsion angles (close to 180°) attest to a coplanar positions of atoms in the $[AuS_2C]$ groups (Table 2). The only exception is one of the rings of cation *A* [Au(1)S(1)S(2)C(1)] in which the deviations of corresponding angles (from 180°) reach 8.3° and 7.5°.

Table 3. Geometric characteristics of Cl···S–C chalcogen–halogen bonds in the structure of **I**

Structural fragment	Cl···S distance, Å	Cl···S–C angle, deg
Cl(2)···S(5)–C(13)	3.259(2)	176.9(2)
Cl(2)···S(6)[a]–C(13)[a]	3.435(2)	179.0(2)
Cl(3)···S(1)–C(1)	3.467(3)	171.8(2)
Cl(3)···S(3)–C(7)	3.312(2)	169.8(2)
Cl(3)···S(7)[b]–C(19)[b]	3.515(3)	163.3(3)
Cl(3)···S(8)–C(19)	3.467(2)	166.8(2)
Cl(4)···S(2)[c]–C(1)[c]	3.271(2)	176.8(2)
Cl(4)···S(4)[c]–C(7)[c]	3.143(2)	173.6(2)

* Symmetry codes: [a] $1-x, -y, 1-z$; [b] $1-x, 2-y, -z$; [c] $-1+x, y, z$.

All PmDtc ligands exhibit typical structural features: (a) double bond character of formally single N–C(S)S bonds (1.291–1.309 Å), which are markedly shorter than the $N-CH_2$ bonds (1.467–1.483 Å); (b) nearly planar C_2NCS_2 moieties (the C–N–C–S torsion angles are close to 0° or 180°, see Table 2). In gold(III) complex cations, heterocyclic $N(CH_2)_5$ moieties, which are stabilized in the chair conformation (C–C bond length is in the 1.501–1.543 Å range), are *trans*-oriented relative to the $[AuS_4]$ chromophore plane.

The anionic part of compound **I** is represented by the binuclear tetrachlorodiargentate(I) ion, $[Ag_2Cl_4]^{2-}$, whose nonequivalent silver atoms, Ag(1) and Ag(2), are linked by two bridging chlorine atoms, Cl(2) and Cl(3), to form a four-membered $[Ag_2Cl_2]$ metallacycle (Fig. 1). The relative positions of the atoms that form this ring are not completely coplanar, as the AgClClAg (–169.34°) and ClAgAgCl (–171.40°) torsion angles somewhat differ from 180° (Table 2). The Ag–Ag interatomic distance in the anion (3.2187 Å)[1] is sub-

[1] It is noteworthy that the distance between the silver atoms in the $[Ag_2Cl_4]^{2-}$ anions varies over a fairly broad range of 3.211–3.659 Å [29–32], which may be due to different contributions (or the absence) of the argenophilic interactions.

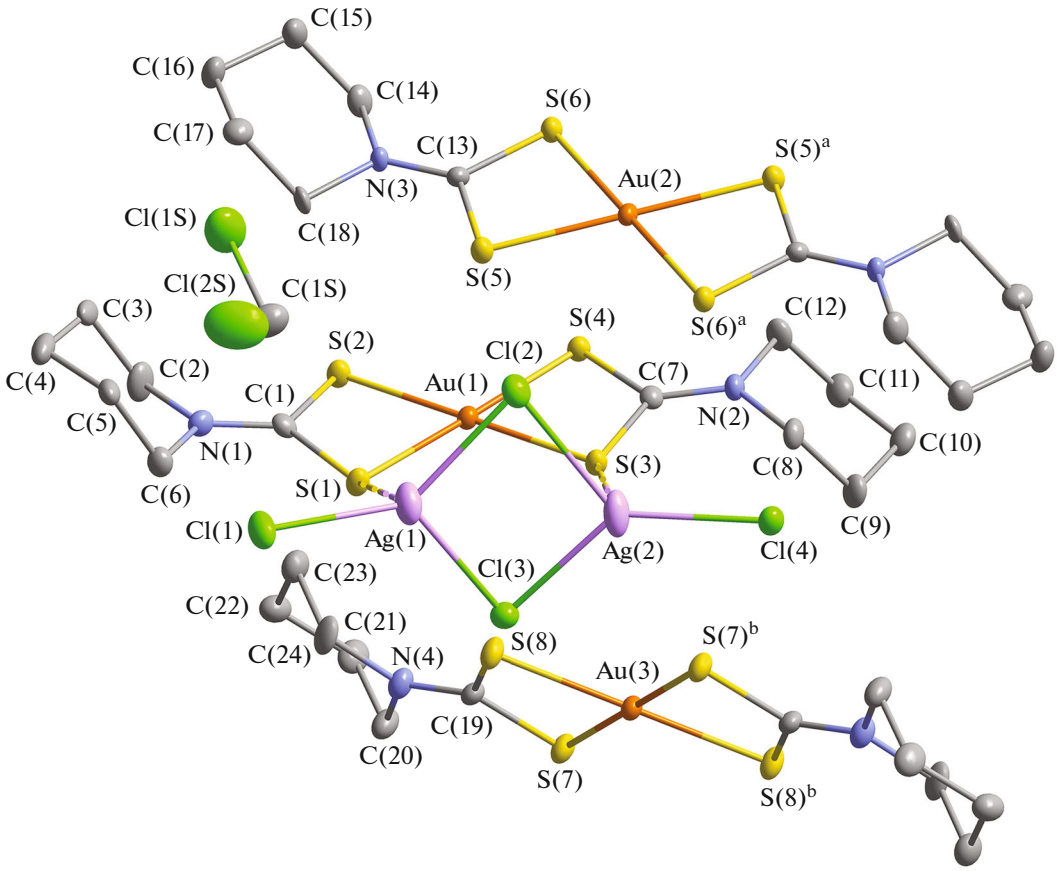

Fig. 1. Structural units of complex **I**: isomeric cations *A* [Au(1)], *B* [Au(2)], and *C* [Au(3)] of $[Au(S_2CNPm)_2]^+$, the $[Ag_2Cl_4]^{2-}$ cyclic anion, and the CH_2Cl_2 solvate molecule (ellipsoids at the 50% probability level). Symmetry codes: [a] $1-x, -y, 1-z$; [b] $1-x, 2-y, -z$.

stantially shorter than twice the van der Waals radius of the silver atom (3.44 Å) [28], which attests to the presence of argentophilic interaction [33], additionally stabilizing the metallacycle. This conclusion is also supported by the type of the rhombic distortion of the $[Ag_2Cl_2]$ ring in which the distance between the opposing silver atoms (see above) is 0.773 Å smaller than that between the chlorine atoms (3.992(3) Å); the angles at the silver atoms are obtuse (103.00° and 101.01°), while the angles at the chlorine atoms are acute (77.85° and 77.35°). Each silver atom also forms a bond with one terminal chlorine atom, Cl(1) or Cl(4) (these bonds are the strongest, see Table 2), thus forming the triple environment for the $[AgCl_3]$ polygons. The Cl(1) and Cl(4) atoms deviate from the mean plane of the $[Ag_2Cl_2]$ ring: the Ag(2)Ag(1)Cl(1) angle is 160.21° and the Ag(1)Ag(2)Cl(4) angle is 169.26°.

The supramolecular self-organization of complex **I** is formed by numerous cation–anion noncovalent Ag···S and Cl···S interactions (Fig. 2). Binuclear tetrachlorodiargentate(I) ions, $[Ag_2Cl_4]^{2-}$, act as a sort of binding sites: each of these ions interacts with all other structural units, including four isomeric gold(III) cations $[Au(S_2CNPm)_2]$ ($2A + B + C$) and the CH_2Cl_2 solvate molecules. The strongest binding is attained with one of cations *A* are a result of pair secondary bonds, Ag(1)···S(1) (2.9456 Å) and Ag(2)···S(3) (3.0055 Å) (Fig. 1), additionally enhanced by pair secondary interactions: Cl(3)···S(3) (3.312 Å) and Cl(3)···S(1) (3.465 Å) (Fig. 2); for comparison, the sums of the van der Waals radii of the corresponding pairs of atoms are 3.52 and 3.55 Å [27, 28]. (The concept of secondary bonds was proposed to describe nonvalent type interactions between atoms at distances comparable with the sums of their van der Waals radii [34].) The $[Ag_2Cl_4]^{2-}$ anion forms a less strong secondary bond, Ag(2)···S(2)^c (3.1833 Å) with the second cation *A*; this bond is, however, supplemented by stronger pair secondary contacts (Cl(4)···S(2)^c, 3.271 Å; and Cl(4)···S(4)^c, 3.143 Å)[2].

[2] Note that in all cases, the length of the identified secondary S···Cl bonds was less than the sum of the van der Waals radii of sulfur and chlorine atoms, and the C–S···Cl angles were in the 163.3°–179.0° range (Table 3). Therefore, according to [35, 36], the obtained structural characteristics imply that the secondary bonds being discussed here can be more definitely classified as chalcogen (chalcogen–halogen) bonds.

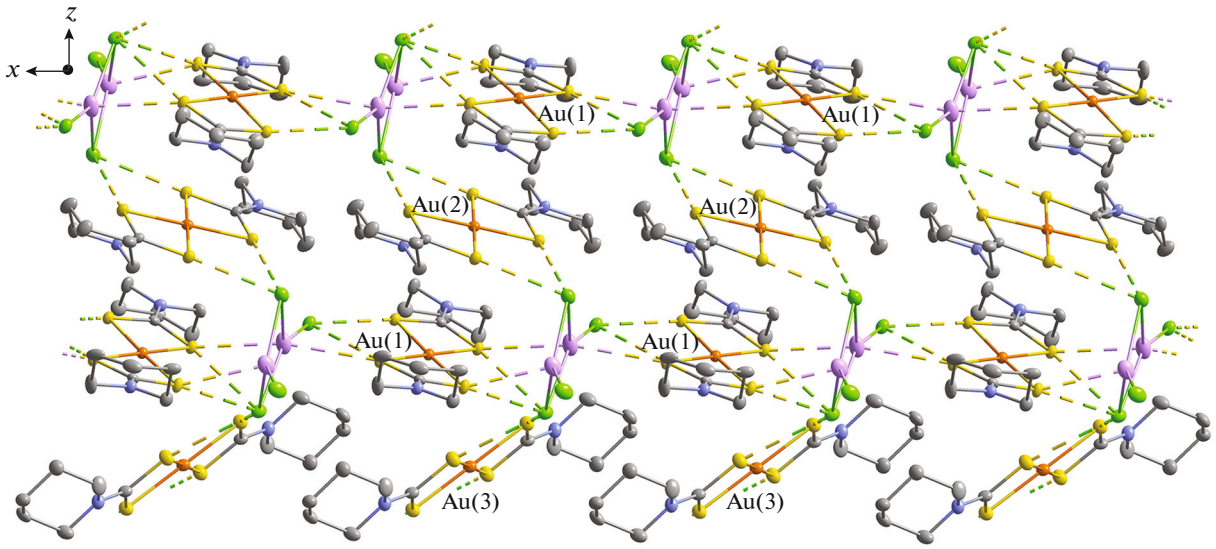

Fig. 2. Construction of pseudopolymer chains $(\cdots[Ag_2Cl_4]\cdots A\cdots)_n$ oriented along the *x* axis and 2D supramolecular layer in the structure of **I**: the secondary interactions Ag···S and Cl···S between the isomeric gold(III) cations: *A* [Au(1)], *B* [Au(2)], and *C* [Au(3)] and $[Ag_2Cl_4]^{2-}$ anions are shown by dashed lines.

Thus, the alternating binuclear silver(I) anions and noncentrosymmetric gold(III) cations *A* form pseudopolymer chains $(\cdots[Ag_2Cl_4]\cdots[Au(S_2CNPm)_2]\cdots)_n$ oriented along the *x* axis (Fig. 2). In these chains, the silver atoms complete their local environment by the secondary Ag···S interactions to distorted polyhedra with displaced vertices, trigonal pyramid $[Ag(1)Cl_3S]$ and trigonal bipyramid $[Ag(2)Cl_3S_2]$.

In turn, the centrosymmetric isomeric gold(III) cations *B* and *C* combine the neighboring supramolecular cation–anion chains $(\cdots\{[Ag_2Cl_4]\cdots A\}^{-}\cdots)_n$ to form a two-dimensional pseudopolymer layer, in which they act as double linkers (Fig. 2). Furthermore, binding of one of neighboring chains is accomplished by only cations *B*, which form pair secondary bonds, $S(5)^{/a}\cdots Cl(2)^{/a}$ (3.259 Å) and $S(6)^{/a}\cdots Cl(2)^{a/}$ (3.435 Å), with the Cl(2) bridging atoms of the anions (Fig. 3). The second neighboring chain is bound only through cations *C*, involving, the Cl(3) bridging atoms; in this case, the least strong pairs of secondary bonds are formed: $S(7)^{b/}\cdots Cl(3)^{/a}$ (3.515 Å) and $S(8)^{/b}\cdots Cl(3)^{/a}$ (3.467 Å). Consideration of the whole set of these S···Cl contacts reveals a second type of zigzag-like pseudopolymer chains, $(\cdots[Ag_2Cl_4]\cdots B\cdots[Ag_2Cl_4]\cdots C\cdots)_n$, directed along the *z* axis (Fig. 3). Finally, other types of weak secondary interactions, S···S, C–H···S, C–H···Cl, C–H···π, and H···H, complete the general binding of the 2D layers, giving rise to 3D supramolecular architecture.

The Cl(1) terminal atom of silver(I) cyclic anion, which is not involved in the formation of 2D supramolecular layers, fixes, together with the Cl(2) bridging atom, the CH_2Cl_2 solvate molecule in **I**, thus forming two nonequivalent C–H···Cl hydrogen bonds (H···Cl, 2.55 and 2.75 Å; C···Cl, 3.518(8) and 3.609(10) Å; ∠C–H···Cl, 165° and 145°, respectively) (Fig. 4).

The thermal behavior of **I** was studied by simultaneous thermal analysis (STA) in which the TG and DSC curves were recorded in parallel (Fig. 5). The course of the TG curve attests to multistage thermal decomposition of the studied complex (Fig. 5*a*). Differentiation of the TG curve revealed the first region (65–194°C), associated with two-stage desolvation of the complex. The total mass loss in this region was 5.63%, which is close to the value calculated for the CH_2Cl_2 molecule (5.74%). It is noteworthy that the separation of the desolvation process (loss of CH_2Cl_2 molecules) into two stages was also observed in our previous study [14]. In the DSC curve (Fig. 5*b*), the loss of solvate molecules is manifested as two low-intensity endotherms at 80.7 and 195.7°C.

Afterwards, the TG curve of complex **I** reaches a steeply descending region of intense thermolysis (~194–306°C) with the main mass loss of 45.31% (Fig. 5*a*). This large loss of mass and presence of inflection points (at 245.0 and 289.0°C) in this region of TG curve attests to a complicated course of thermolysis of **I**, which leads to reduction of gold(III) to the elemental state (in the cation) and release of AgCl (in the anion), with the calculated mass loss being 48.20%. The respective part of the DSC curve includes an endotherm with a peak at 202.7°C (Fig. 5*b*), which should be attributed to melting of the desolvated form of **I** (the extrapolated T_m is 198.9°C). An independent determination of the melting point of the nonsolvated complex **I** in a glass capillary con-

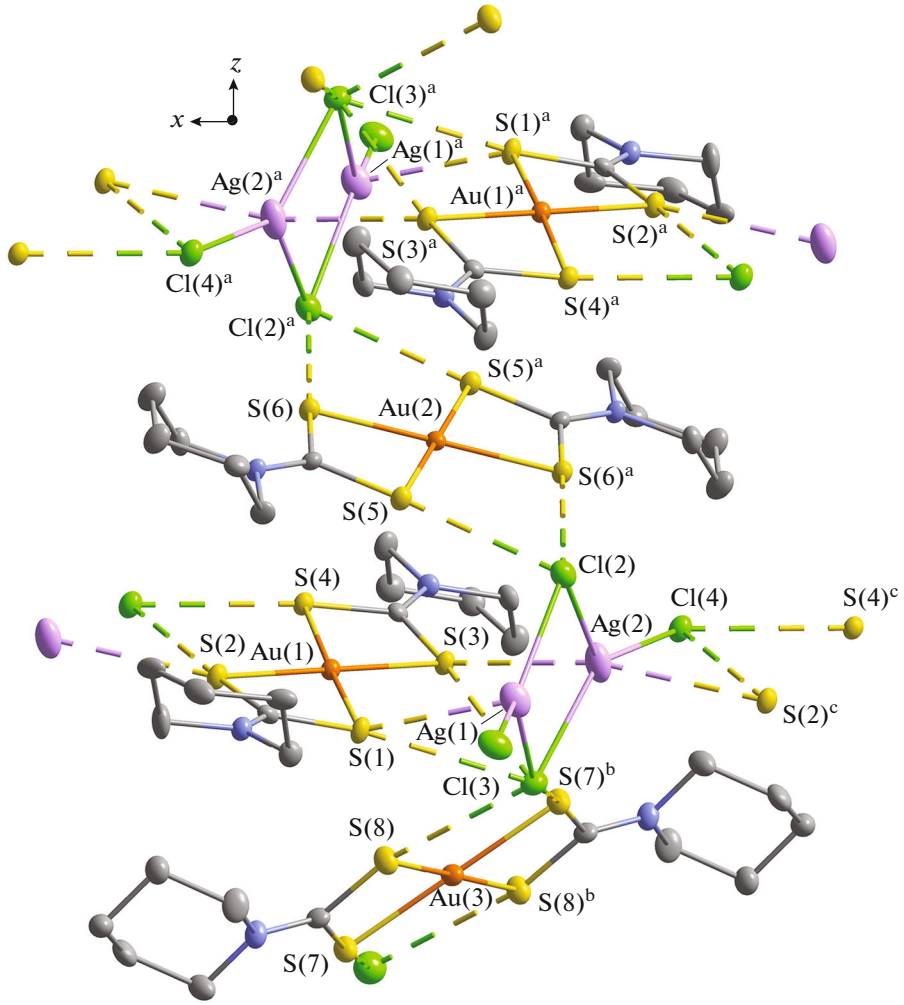

Fig. 3. Mode of binding of neighboring pseudopolymer chains $(\cdots[Ag_2Cl_4]\cdots A\cdots)_n$ with participation of isomeric gold(III) cations *B* and *C*; construction of zigzag-like pseudopolymer chain of the $(\cdots[Ag_2Cl_4]\cdots B\cdots[Ag_2Cl_4]\cdots C\cdots)_n$ type along the *z* axis. The secondary interactions Cl···S and Ag···S are shown by dashed lines. Symmetry codes: [a] $1-x, -y, 1-z$; [b] $1-x, 2-y, -z$; [c] $-1+x, y, z$.

firmed this conclusion: melting with decomposition (vigorous gas evolution) was established in the 200–202°C range. The region of DSC curve being discussed includes two more endotherms at 237.0 and 276.0°C (the extrapolated temperatures of the processes are 220.1 and 261.4°C), each being projected on the corresponding region of intense thermolysis of the TG curve (Figs 5*b*, 5*c*).

The two subsequent slightly sloping regions of mass loss (Fig. 5*a*) are associated with the reduction of silver(I) to the elemental state (the mass loss is 4.76%; the calculated value is 4.79%) and the smooth final desorption of volatile thermolysis products with a mass loss of 4.96%. The residual mass at 1100°C is 39.73%, which is somewhat lower than the calculated value for the reduced gold and silver (41.26%). After completion of the measurements, light yellow beads of a gold–silver alloy were detected on the bottom of the corundum crucible (Fig. 5*d*); the extrapolated T_m of this alloy (1033.4°C) was found from the high-temperature endotherm at 1037.1°C (Fig. 5*b*). This value is in good agreement with extrapolated T_m values of the Au–Ag alloys obtained from other complexes ($[Au(S_2CNEt_2)_2][AgCl_2]$, 1031.8°C [18]; $[Au(S_2CNPr_2)_2][AgCl_2]$, 1030.4°C [19]; $[Au(S_2CN^iBu_2)_2][AgCl_2]$, 1029.7°C [16]), which are also characterized by 1 : 1 ratio of the metals. Whereas, the alloys obtained from complexes with Au : Ag ratio of 2 : 1 have markedly higher extrapolated T_m values: 1046.2°C ($[Au(S_2CNEt_2)_2]_2[AgCl_2]Cl\cdot 2H_2O$ [18]) and 1040.2°C ($[Au\{S_2CN(CH_2)_6\}_2]_2[AgCl_2]Cl\cdot 2CHCl_3$ [20]).

The antibacterial activity of complex **I** was studied against the nonpathogenic *M. smegmatis* strain. It is known that the chemotherapeutic drug resistance of mycobacteria is due to low permeability of the mycobacterial cell wall, associated with specific features of its structure. Fast growing nonpathogenic *M. smegmatis* strain is used to model slowly growing *M. tuberculosis* and also for primary screening of anti-tuberculosis

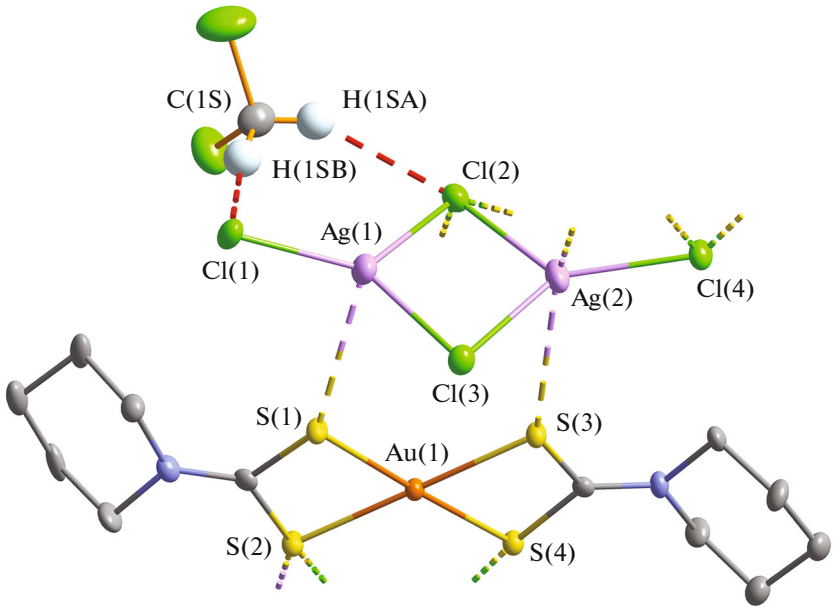

Fig. 4. Nonequivalent C–H···Cl hydrogen bonds formed by the CH_2Cl_2 solvate molecule with the anion–cation pair $\{[Ag_2Cl_4]\cdots A\}^-$. The hydrogen bonds and the secondary interactions Ag···S and Cl···S are shown by dashed lines.

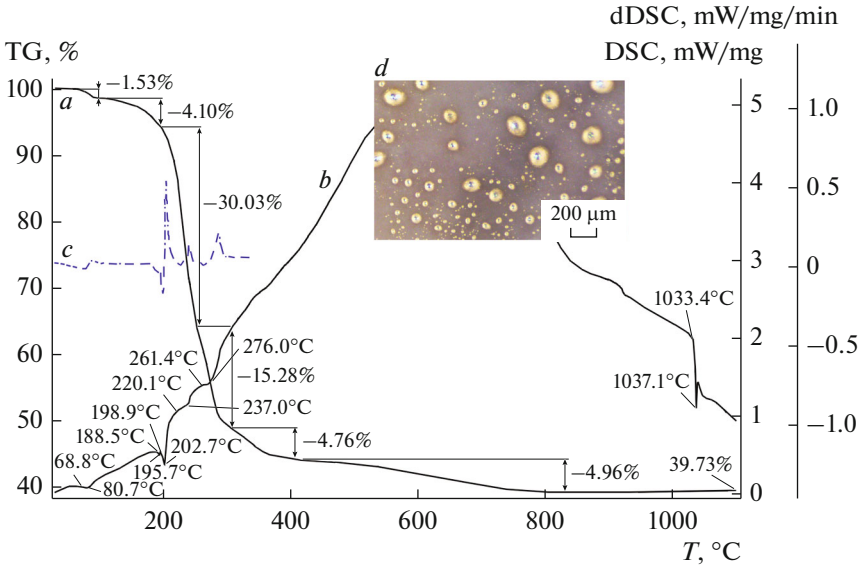

Fig. 5. (*a*) TG and (*b*) DSC curves and (*c*) low-temperature part of dDSC curve of complex **I**. (*d*) Photograph of the crucible bottom with Au–Ag alloy beads after completion of the thermolysis.

drugs [37, 38]. It follows from the data in Table 4 that the double Au(III)–Ag(I) dithiocarbamato-chlorido complex exhibits significantly higher biological activity than Rif, a first-line drug for the treatment of tuberculosis. It is noteworthy that the activity of the initial sodium salt NaPmDtc is also relatively high and comparable with that of Rif (Table 4). It is known that the complex formation of bioactive compounds with both essential (Cu^{2+}, Co^{3+}, Fe^{3+}) and noble (e.g., Ag^+) metal cations can substantially enhance the inhibition of the viability of microorganisms, including mycobacteria [7, 39–46]. Compound **I** was found to exhibit particularly this effect: the MIC value is almost ninety times lower than that of the initial ligand salt and a hundred times lower than that of Rif (Table 4). It is worth noting that the inhibition zone formed under pressure of complex **I** is not overgrown with time (unlike that of the initial ligand salt), which attests to long-term bacteriostatic effect against the mycobacterial strain.

Table 4. Antibacterial activity *in vitro* of **I** against *M. smegmatis**

Compound	MIC, μg/disc	Inhibition zone, mm	
	24 h	24 h	120 h
I	0.05	6.8 ± 0.3	6.4 ± 0.1
NaPmDtc	4.6	6.4 ± 0.1	6.1 ± 0.1**
Rif	5	7.2 ± 0.3	7.0 ± 0.0

* The paper disc diameter is 6 mm.

** The inhibition zone of *M. smegmatis mc^2 155* is overgrown.

Thus, a new double pseudopolymer Au(III)–Ag(I) complex, $[Au\{S_2CN(CH_2)_5\}_2]_2[Ag_2Cl_4]\cdot CH_2Cl_2$, was prepared and characterized in detail by X-ray diffraction, IR spectroscopy, and STA. It was shown that the compound has an intricate supramolecular structure formed via multiple secondary interionic interactions (Au···S, Cl···S) and hydrogen bonds (C–H···Cl). The complex exhibits a high biological activity *in vitro* against nonpathogenic *M. smegmatis* strain, including the long-term bacteriostatic effect. Study of the thermal behavior of **I** revealed conditions for the quantitative recovery of metals (Au, Ag) present in the complex.

ACKNOWLEDGMENTS

Elemental analysis and IR spectroscopy were performed using equipment of the Center for Collective Use of Physical Investigation Methods of the Kurnakov Institute of General and Inorganic Chemistry, Russian Academy of Sciences. X-ray diffraction experiments were carried out at the Center of Molecular Structure Investigations of the Nesmeyanov Institute of Organoelement Compounds, Russian Academy of Sciences.

CONFLICT OF INTEREST

The authors declare that they have no conflicts of interest.

REFERENCES

1. Massoud, A.A., Hefnawy, A., Langer, V., et al., *Polyhedron*, 2009, vol. 28, no. 13, p. 2794.
2. Tang, X., Qi, C., He, H., et al., *Adv. Synth. Catal.*, 2013, vol. 355, no. 10, p. 2019.
3. Trivedi, M., Singh, G., Kumar, A., and Rath, N.P., *Inorg. Chim. Acta*, 2015, vol. 438, p. 255.
4. Ehsan, M.A., Khaledi, H., Tahir, A.A., et al., *Thin Solid Films*, 2013, vol. 536, p. 124.
5. Mothes, R., Jakob, A., Waechtler, T., et al., *Eur. J. Inorg. Chem.*, 2015, no. 10, p. 1726.
6. Lutze, O., Meruva, R.K., Ramamurthy, A.F.N., et al., *J. Anal. Chem.*, 1999, vol. 364, p. 41.
7. Montelongo-Peralta, L.Z., León-Buitimea, A., Palma-Nicolás, J.P., et al., *Sci. Rep.*, 2019, vol. 9, 5471.
8. Hesse, R. and Nilson, L., *Acta Chem. Scand.*, 1969, vol. 23, no. 3, p. 825.
9. Jennische, P. and Hesse, R., *Acta Chem. Scand.*, 1971, vol. 25, no. 2, p. 423.
10. Anacker-Eickhoff, H., Hesse, R., Jennische, P., and Wahlberg, A., *Acta Chem. Scand.*, 1982, vol. 36, no. 3, p. 251.
11. Zhang, W.-G., Zhong, Y., Tan, M.-Y., et al., *Chin. J. Chem.*, 2002, vol. 20, no. 5, p. 420.
12. Song, Y.-W., Yu, Z., and Zhang, Q.-F., *Acta Crystallogr., Sect. C: Cryst. Struct. Commun.*, 2006, vol. 62, no. 5, p. m214.
13. Yin, X., Xie, M.-B., Zhang, W.-G., and Fan, J., *Acta Crystallogr., Sect. E: Struct. Reports Online*, 2007, vol. 63, no. 9, p. m2273.
14. Korneeva, E.V., Ivanov, A.V., Gerasimenko, A.V., et al., *Russ. J. Gen. Chem.*, 2019, vol. 89, no. 8, p. 1642. https://doi.org/10.1134/S1070363219080152
15. Ajibade, P.A. and Botha, N.L., *J. Sulf. Chem.*, 2020, vol. 41, no. 6, p. 657.
16. Korneeva, E.V., Smolentsev, A.I., Antzutkin, O.N., and Ivanov, A.V., *Inorg. Chim. Acta*, 2021, vol. 525, 120383.
17. Oladipo, S.D. and Omondi, B., *Molbank*, 2022, vol. 2022, no. 1, M1327.
18. Korneeva, E.V., Loseva, O.V., Smolentsev, A.I., and Ivanov, A.V., *Russ. J. Gen. Chem.*, 2018, vol. 88, no. 8, p. 1680. https://doi.org/10.1134/S1070363218080200
19. Korneeva, E.V., Smolentsev, A.I., Antzutkin, O.N., and Ivanov, A.V., *Russ. Chem. Bull.*, 2019, vol. 68, no. 1, p. 40. https://doi.org/10.1007/s11172-019-2413-7
20. Korneeva, E.V., Novikova, E.V., Loseva, O.V., et al., *Russ. J. Coord. Chem.*, 2021, vol. 47, no. 11, p. 769. https://doi.org/10.1134/S1070328421090050
21. Liu, W., Zhang, J., Peng, Z., et al., *Coll. Surf. A*, 2018, vol. 544, p. 111.
22. Yang, J. and Ying, J.Y., *Chem. Commun.*, 2009, no. 22, p. 3187.
23. Byr'ko, V.M., *Ditiokarbamaty* (Dithiocarbamates), Moscow: Nauka, 1984.
24. Sheldrick, G.M., *Acta Crystallogr., Sect. A: Found. Adv.*, 2015, vol. 71, no. 1, p. 3.
25. Dolomanov, O.V., Bourhis, L.J., Gildea, R.J., et al., *J. Appl. Crystallogr.*, 2009, vol. 42, no. 2, p. 339.
26. Gremlikh, G.U. *Yazyk spektrov. Vvedenie v interpretatsiyu spektrov organicheskikh soedinenii* (Language of

Spectra. Introduction to Interpretation of Spectra of Organic Compounds), Moscow: LLC Bruker Optik, 2002.

27. Bondi, A., *J. Phys. Chem.*, 1964, vol. 68, no. 3, p. 441.
28. Bondi, A., *J. Phys. Chem.*, 1966, vol. 70, no. 9, p. 3006.
29. Helgesson, G. and Jagner, S., *Dalton Trans.*, 1988, no. 8, p. 2117.
30. Helgesson, G. and Jagner, S., *Dalton Trans.*, 1990, no. 8, p. 2413.
31. Hassan, A., Breeze, S.R., Courtenay, S., et al., *Organometallics*, 1996, vol. 15, no. 26, p. 5613.
32. Aboulkacem, S., Tyrra, W., and Pantenburg, I., *J. Chem. Cryst.*, 2006, vol. 36, no. 2, p. 141.
33. Schmidbaur, H. and Schier, A., *Angew. Chem., Int. Ed. Engl.*, 2015, vol. 54, no. 3, p. 746.
34. Alcock, N.W., *Adv. Inorg. Chem. Radiochem.*, 1972, vol. 15, no. 1, p. 1.
35. Wang, W., Ji, B., and Zhang, Y., *J. Phys. Chem. A*, 2009, vol. 113, no. 28, p. 8132.
36. Scilabra, P., Terraneo, G., and Resnati, G., *Acc. Chem. Res.*, 2019, vol. 52, no. 5, p. 1313.
37. Ramón-García, S., Ng, C., Anderson, H., et al., *Antimisrob. Agents Chemother.*, 2011, vol. 55, no. 8, p. 3861.
38. Bekker, O.B., Sokolov, D.N., Luzina, O.A., et al., *Med. Chem. Res.*, 2015, vol. 24, no. 7, p. 2926.
39. Lutsenko, I.A., Baravikov, D.E., Kiskin, M.A., et al., *Russ. J. Coord. Chem.*, 2020, vol. 46, no. 6, p. 411. https://doi.org/10.1134/S1070328420060056
40. Lutsenko, I.A., Baravikov, D.E., Kiskin, M.A., et al., *Russ. J. Coord. Chem.*, 2020, vol. 46, no. 12, p. 787. https://doi.org/10.1134/S1070328420120040
41. Lutsenko, I.A., Yambulatov, D.S., Kiskin, M.A., et al., *Chem. Select.*, 2020, vol. 5, no. 38, p. 11837.
42. Melnic, S., Prodius, D., Stoeckli-Evans, H., et al., *Eur. J. Med. Chem.*, 2010, vol. 45, no. 4, p. 1465.
43. Lutsenko, I.A., Kiskin, M.A., Koshenskova, K.A., et al., *Russ. Chem. Bull.*, 2021, vol. 70, no. 3, p. 463. https://doi.org/10.1007/s11172-021-3109-3
44. Uvarova, M.A., Lutsenko, I.A., Kiskin, M.A., et al., *Polyhedron*, 2021, vol. 203, 115241.
45. Lutsenko, I.A., Nikiforova, M.E., Koshenskova, K.A., et al., *Russ. J. Coord. Chem.*, 2021, vol. 47, no. 12, p. 881. https://doi.org/10.1134/S1070328421350013
46. Lutsenko, I.A., Baravikov, D.E., Koshenskova, K.A., et al., *RSC Adv.*, 2022, vol. 12, no. 9, p. 5173.

Translated by Z. Svitanko